An electrical analogy for the Pentland Firth tidal stream power resource

An Electrical Analogy for the Pentland Firth Tidal Stream Power Resource

Submitted to *Proceedings of the Royal Society Part A* on 30/03/2013.

Resubmitted on 3/09/2013.

Accepted on 2/10/2013.

Scott Draper
Centre for Offshore Foundation Systems,
University of Western Australia,
Crawley, 6009,
Australia.

Thomas A. A. Adcock
Department of Engineering Science,
University of Oxford,
Parks Road,
Oxford OX1 3PJ, U.K.

Alistair G.L. Borthwick
School of Engineering,
University of Edinburgh,
Kings Buildings
Edinburgh EH9 3JL, U.K

Guy T. Houlsby
Department of Engineering Science,
University of Oxford,
Parks Road,
Oxford OX1 3PJ, U.K.

Figures: 6
Tables: 6
Words: 6,672

Abstract

Several locations in the Pentland Firth have been earmarked for the deployment of separate farms of tidal turbines. However, recent numerical modelling suggests that these farms will be inter-dependent and that they must work together to optimise their collective performance (see Draper *et al.* 2013). To explain this inter-dependence, in the present paper we develop an electrical circuit analogy to describe flow through the Pentland Firth, in which parallel connections in the circuit represent different sub-channels formed by the islands of Swona, Stroma and the Pentland Skerries. The analogy is introduced in stages, beginning with turbines placed in a single channel, then turbines placed in a sub-channel connected in parallel to another sub-channel, and finally more complicated arrangements in which turbines are installed both in parallel and in series within a multiply-connected channel. The analogy leads to a general formula to predict the tidal power potential of turbines placed in a sub-channel connected in parallel to another sub-channel, and a predictive model for more complicated multiply-connected channel arrangements. Power estimates made using the formula and predictive model (which may be applied using only measurements of the undisturbed natural tidal hydrodynamics) are shown to agree well with numerical model predictions for the Pentland Firth, providing useful insight into how best to develop the resource.

Keywords: Tidal stream power, Pentland Firth, Shallow water flow.

1. Introduction

The Pentland Firth, UK, is a well-known candidate site for tidal stream power generation. In a recent paper, Draper *et al.* (2013) used a numerical model based on the shallow water equations to estimate the maximum power that can be removed by placing turbines across the entire Pentland Firth and, independently, across the sub-channels formed by the islands of Swona, Stroma and the Pentland Skerries (see Figure 1a for locations). For the entire Firth Draper *et al.* estimated a power potential (averaged over the tidal cycle) of 4.2 GW accounting for both M2 and S2 tidal constituents, which they found to agree reasonably well with a prediction from an existing theoretical model for turbines placed in a tidal channel due to Garrett and Cummins (2005) (hereafter GC05). However, when turbines are placed across each of the sub-channels Draper *et al.* found that the maximum power which can be extracted from one sub-channel depends on the operation (or otherwise) of tidal turbines placed in parallel sub-channels or in series along the Firth. This finding underlines a complexity to the Pentland Firth tidal resource and importantly suggests that different developers must work cooperatively when deciding where best to locate farms of turbines in the sub-channels, or when deciding on how to operate tidal turbines at the sites earmarked by the Crown Estate (2011).

The complexity of the Pentland Firth tidal power resource is similar to that reported by Sutherland *et al.* (2007) for Johnstone Strait, Canada, and Polagye and Malte (2009) for several idealised tidal channels. In each of these studies numerical models were used to show that the power removed by tidal turbines placed across a sub-channel could be significantly reduced if parallel sub-channels existed; however neither study provided a theoretical model to predict this reduction. More recently Atwater and Lawrence (2010) studied an idealised multiply-connected channel consisting of two sub-channels connected in parallel and demonstrated a similar reduction in power potential. In contrast to the earlier work Atwater and Lawrence also presented a predictive formula for power extraction, however this formula assumed that the tidal flow is quasi-steady; i.e. the flow rate is in phase with the time varying free surface elevation difference across the multiply-connected channel. Direct application of the Atwater and Lawrence (2010) model to make predictions for the Pentland Firth is therefore difficult to justify because the flow through the Firth is not quasi-steady (Draper *et al.* (2013)). Furthermore, Atwater and Lawrence (2010) provided no guidance on how to treat scenarios in which tidal turbines are placed in more than one location within the channel or scenarios involving more than two sub-channels.

With this in mind, the aim of the present paper is to provide insight into the apparent complexity of the tidal resource in the Pentland Firth, and multiply-connected channels more generally, through the development of a predictive theoretical model that is valid for (i) multiply-connected channels in which tidal flow may or may not be quasi-steady, (ii) scenarios when tidal turbines are placed in more than one location within the channel, and (iii) multiply-connected channels with more than two sub-channels. To develop the theoretical model we have drawn on a revealing characteristic of the numerical results obtained by Draper *et al.* (2013). This characteristic is that the flow of water through the Pentland Firth appears to be analogous to current flowing through an electrical circuit, with the sub-channels formed by the islands of Swona, Stroma and the Pentland Skerries representing parallel connections in the circuit. For example, the numerical results indicate that when tidal turbines are placed between the islands of Swona and Stroma, the flows to the north of Stroma and to the south of Swona increase (see Case C in Table 2). Consequently the flow through the central sub-channel is reduced, in an analogous manner to how the current would reduce through a resistor connected in parallel when its resistance is increased.

Guided by this observation we adopt an electrical circuit analogy in this paper and use it to estimate power extraction from multiply-connected channels. To make the approach as general as possible, we start by developing the electrical circuit analogy in the context of the single tidal channel model presented by GC05. Next we extend the analogy to assess the power potential of one sub-channel connected in parallel to another sub-channel, and finally we consider the more general arrangement in which tidal turbines are placed both in series and in parallel within a multiply-connected channel. For the last two stages we apply the analogy to the Pentland Firth and make comparisons between theoretical predictions drawn from the electrical analogy and the numerical model results of Draper *et al.* (2013).

It should, of course, be noted that our use of an electrical circuit analogy to describe shallow water flow is not new. Miles (1971) used an electrical circuit to analyse the surface wave response of a harbour and Lighthill (1978) provided a detailed discussion on the application of the electrical analogy to flow in channels. More recently Rainey (2009) and Cummins (2013) respectively used the electrical analogy to interpret the tidal power potential of the Severn Estuary and of parallel inlets leading to an idealised enclosed basin. The analysis presented herein for parallel sub-channels is consistent with that of Cummins (2013), although it should be noted that the predictive formula derived in Section 3.2 of the present paper is unique in that it represents the power potential in terms of undisturbed hydrodynamic quantities; specifically the volume flow rate through the channel and elevation differences across the channel.

The remainder of the paper is structured as follows. Firstly Section 2 briefly presents the results from a 2D shallow water numerical model used by Draper *et al.* (2013) to estimate the power potential of the Pentland Firth as a whole, and of its sub-channels. Next Section 3 describes the application of the electrical analogy to the single channel model of GC05, followed by turbines installed in a parallel sub-channel, and finally turbines deployed in parallel and in series within a multiply-connected channel; with comparisons made to Draper *et al.* (2013) where relevant. Section 4 presents the main conclusions.

2. Power Potential of the Pentland Firth

Draper *et al.* (2013) explore the power potential of the Pentland Firth using a depth-averaged numerical model. Specifically, they estimate the maximum power that can be extracted by placing a row of turbines across the Pentland Firth, and various combinations of the sub-channels formed by the islands of Swona, Stroma and the Pentland Skerries. Tables 1 and 2 reproduce the key results obtained by Draper *et al.* Table 1 presents the maximum power (averaged over a tidal cycle) removed by one or more 'strips' of added bed roughness representing fence(s) of tidal turbines. These strips are outlined in Figure 1b together with the numerical mesh used within the Pentland Firth to simulate tidal currents. Table 2 gives the fractional change in amplitude of flow rate through the Pentland Firth (at A) and the sub-channels at maximum average power extraction, compared with natural conditions. Table 2 also gives the fractional change in elevation difference either side of the Pentland Firth (defined as a in the caption) for the same conditions.

Implications of the estimates in Table 1 and Table 2 have been discussed by Draper *et al.* (2013). The present paper provides further insight into these results, so as to assist regulators in developing the tidal resource of the Pentland Firth and other candidate sites involving similar multiply-connected channel systems.

3. An equivalent circuit analysis of a tidal channel

3.1 Tidal fences placed in a single tidal channel

To introduce the electrical analogy we begin by reviewing the model of GC05 for tidal turbines installed across a single isolated tidal channel (Figure 2a). GC05 model the flow through a tidal channel using the one-dimensional shallow water approximation to the momentum equation

$$\frac{\rho}{A}\frac{\partial Q}{\partial t}+\frac{\rho Q}{A}\frac{\partial}{\partial x}\left(\frac{Q}{A}\right)+\rho g\frac{\partial \zeta}{\partial x}=-\rho\left(\frac{C_d}{hA^2}+\delta\right)Q|Q|, \tag{1}$$

where $Q(x,t)$ is the one-dimensional flow rate through the channel, x is distance along the channel, t is time, $\zeta(x,t)$ is the free surface elevation, ρ is water density (taken as 1027 kg/m^3 throughout), g is acceleration due to gravity, $A(x)$ is the cross-sectional area of the channel (assumed constant over the tidal cycle), $h(x)$ is the average water depth at any point along the channel (also assumed constant over the cycle), C_d is a drag coefficient parameterising background friction in the channel, and δ is a resistance introduced to represent tidal turbines placed across the width of the channel. The definition of this resistance implies that the power extracted from the channel by turbines, averaged over a tidal period T, is $\bar{P}=(\rho\int_0^T \delta|Q|^3\,dt)/T$.

To simplify Equation (1) GC05 assume that the channel is short compared to the characteristic tidal wavelength, so that the flow rate will be approximately the same everywhere along the channel (as is the case for the Pentland Firth; see Draper *et al.* 2013). Equation (1) can thus be integrated along the channel length l and rearranged to give

$$\rho g\xi_0=\rho c\frac{dQ}{dt}+\rho\delta Q|Q|+\rho\left(\frac{1}{2A_l^2}-\frac{1}{2A_0^2}+\int_0^l\frac{C_d}{hA^2}dx\right)Q|Q|, \tag{2}$$

where $c=\int_0^l A^{-1}\,dx$, $\xi_0=\xi(0,t)-\xi(l,t)$ is the time-varying elevation (or 'head') difference either side of the channel, and the parameters A_l and A_0 define the cross-sectional areas at the exit and entrance of the channel, respectively. These latter parameters, although difficult to define individually, can be combined with the unknown bed friction in the channel. Equation (2) then becomes

$$\rho g\xi_0=\rho c\frac{dQ}{dt}+(\rho\delta|Q|+\rho\delta_1|Q|)Q, \tag{3}$$

in which δ_1 now captures all the natural sources of energy loss in the channel which are proportional to the square of the flow rate (we will refer to this collective term as 'drag'). Equation (3) illustrates that the dynamic pressure (left hand term) is responsible for both accelerating flow through the channel and performing work against natural drag and the operation of tidal tubrines (GC05). GC05 assume that the dynamic pressure does not change when turbines are added to the channel, which simplifies the analysis. They then solve Equation (3) directly for various channel geometries (defined by c and δ_1) and determine the maximum power extraction; leading eventually to the general result:

$$\overline{P}_{max}=\gamma\rho g a Q_p, \tag{4}$$

where $\overline{P}_{max}$ is the power potential of the tidal channel (i.e. the maximum power that can be extracted, averaged over a tidal cycle) and is dependent on the peak undisturbed flow rate through the channel Q_p and the amplitude of the dynamic head across the channel a (which, as noted above, is assumed to remain unchanged with the addition of tidal turbines). The multiplier γ depends on the phase lag of the flow rate behind the driving head (GC05).

An alternative method to investigate Equation (3) is to adopt an electrical circuit analogy. To introduce this analogy, Equation (3) can be compared with

$$V = L\frac{dI}{dt} + RI, \tag{5}$$

which describes the time varying current I in an electric circuit with inductance L, resistance R, and driving voltage V. Adopting $Q \equiv I$, direct comparison with Equation (3) thus implies that the dynamic pressure can be interpreted as the voltage driving the flow through the channel (*i.e.* $V \equiv \rho g \xi_0$) and the mass of water in the channel introduces an inductance $L = \rho c$. The natural drag and tidal turbines represent non-linear resistors that depend on flow rate, with $R_1 = \rho \delta_1 |Q|$ and $R_t = \rho \delta |Q|$ respectively. Using these definitions, a single tidal channel is therefore equivalent to the electrical circuit in Figure 2b.

With the adoption of the electrical circuit analogy, GC05's assumption that the dynamic pressure does not change with the addition of turbines simply implies that the applied voltage remains unchanged. Addition of turbines to increase R_t, and hence the effective impedance in the circuit, must therefore lead to a reduction in the current flowing through the circuit (and hence the flow rate in the channel). From the electrical analogy it is therefore easy to see that tidal turbines reduce the flow rate through the channel which, in turn, implies the existence of an optimum value of power extraction (GC05).

Maximisation of the power removed by tidal turbines is equivalent to optimising the power dissipated in the resistor representing the turbines. For an electrical circuit with linear resistors this optimisation is a well-known problem and leads to the familiar requirement of impedance matching, in which the resistance of the turbines should be set equal to the magnitude of the natural impedance in the channel (*e.g.* Rainey, 2009). For example, if we consider $V_0 = \rho g \xi_0 = Re\{\rho g a e^{i\omega t}\}$ and initially assume that the resistances R are independent of the flow rate (*i.e.* linear), then the optimum tidal device resistance is simply $R_{t,opt} = |Z_1| = ((\omega L_1)^2 + R_1^2)^{1/2}$, where $Z_1 = i\omega L_1 + R_1$ is the natural impedance of the channel. The maximum power (averaged over a tidal cycle) can then be written as:

$$\overline{P}_{max} = \frac{1}{4}\left(\frac{1}{1 + R_1/|Z_1|}\right)|V_0||I_0| = \frac{1}{4}\left(\frac{1}{1 + R_1/|Z_1|}\right)\rho g a Q_p, \tag{6}$$

where the subscript '0' refers to quantities before tidal turbines are introduced (*i.e.* when $R_t = 0$) and Q_p is the magnitude of the undisturbed flow rate (*i.e.* $|I_0| \equiv |Q_0| = Q_p$). Equation (6) indicates that for a channel with drag-dominated impedance ($R_1/|Z_1| \to 1$) and a channel with no natural drag ($R_1/|Z_1| \to 0$), the optimum power ranges from $0.125\rho g a Q_p$ to $0.25\rho g a Q_p$, respectively. Hence the optimum power is dependent on dynamic pressure, peak natural flow rate, and the proportion of the channel's impedance due to drag. We note that a similar result to (6) is presented by Cummins (2013), but in a different form.

It is simple to alter the result in Equation (6) to allow for the non-linear dependence of the resistors on the flow rate, and doing so leads directly to Equation (4). Clearly the form of Equation (4) is very similar to Equation (6); in the non-linear case the multiplier γ depends

on a single parameter $\lambda = ga\delta_1/(c\omega)^2$, which also describes the proportion of the channel's impedance due to drag (but includes the dynamic head because of the non-linear dependence on flow rate). For inertia-dominated channels with no natural drag ($\lambda \to 0$) it can be shown that $\gamma \to 0.24$, whereas for a channel dominated by natural drag ($\lambda \to \infty$) it can be shown that $\gamma \to 0.19$ (GC05); this is higher than the fraction of 0.125 for the linear case in Equation (6) because the natural impedance of the channel reduces as turbines are added (due to the dependence of the natural resistance on flow rate), and so the dynamic pressure driving flow through the channel can do relatively more work on the tidal turbines.

Before extending our analysis to multiply-connected channels it is also interesting to note that for single channels the electrical analogy highlights that at least two of the three parameters – natural flow rate (current), dynamic driving pressure (voltage), or channel geometry and natural drag (natural impedance) – are needed to define completely the channel (circuit) in the natural state and, in turn, calculate the power potential of the channel. Hence kinetic flux in isolation, which may be used to infer only the flow rate in the channel in the absence of turbines, is not sufficient to estimate power potential (explaining the doubt concerning the estimate made by Black and Veatch (2005), and discussed in the context of the Pentland Firth by Draper *et al.* (2013)). Likewise, the metric of natural dissipation, which has also been used to interpret the tidal stream resource (DTI, 2004), is not sufficient because it only provides information on the natural resistance (not total impedance) coupled with flow rate in the channel. In contrast to the metrics of kinetic flux and natural power dissipation, Equation (4) includes both the flow rate (current) and the driving pressure (voltage).

3.2 Tidal fences placed in parallel sub-channels

We now consider the problem of fences of tidal turbines placed across a sub-channel that is located within a simple multiply-connected channel (see Figure 3a). To do this we begin by assuming that the tidal range is small and the entire channel system is compact (so that the flow rate within the channel is approximately the same everywhere along the channel; i.e. the flow is assumed to be non-divergent). The shallow water approximation to the momentum equation can then be integrated along various sections of the channel, leading to the system:

$$\rho c_1 \frac{dQ}{dt} = \rho g\, \xi_0 - \rho\delta_1 |Q| Q - \rho g \xi_2, \tag{7a}$$

$$\rho c_2 \frac{dQ_2}{dt} = \rho g \xi_2 - \rho\delta_2 |Q_2| Q_2 - \rho\delta |Q_2| Q_2, \tag{7b}$$

$$\rho c_3 \frac{dQ_3}{dt} = \rho g \xi_2 - \rho\delta_3 |Q_3| Q_3. \tag{7c}$$

where $c_1 = \int_0^{l_1} A^{-1}\, dx + \int_{l_1+l_2}^{l_1+l_2+l_3} A^{-1} dx$, $c_2 = \int_{l_1}^{l_1+l_2} A_2^{-1}\, dx$, $c_3 = \int_{l_1}^{l_1+l_2} A_3^{-1}\, dx$, the intermediate lengths l_1, l_2 and l_3 are nominally defined in Figure 3a (note the lengths of the sub-channels could, in general, be different), and $A(x)$, $A_2(x)$ and $A_3(x)$ are the cross-sectional areas of the main channel and sub-channels, respectively. In Equation (7) the parameter ξ_0 now describes the dynamic head difference across the entire multiply-connected channel system, ξ_2 is the dynamic head difference across the sub-channels, δ is a parameter defining the resistance offered by tidal turbines (assumed to be placed in Sub-channel 2), and the parameters δ_1, δ_2 and δ_3 describe the natural drag in individual sections of the channel. Finally, Q is the total flow rate through the channel system and is, by definition, equal to the sum of the flow rates through Sub-channel 2, defined as Q_2, and the remaining sub-channel, defined as Q_3.

Taking $I \equiv Q$ Equation (7) is now equivalent to the parallel circuit in Figure 3c with the main connecting channel having inductance $L_1 = \rho c_1$ and resistance $R_1 = \rho\delta_1|Q|$, whilst the smaller sub-channels have inductance $L_2 = \rho c_2$ and $L_3 = \rho c_3$, and resistances $R_2 = \rho\delta_2|Q_2|$ and $R_3 = \rho\delta_3|Q_3|$, respectively. The dynamic pressure difference across the entire channel is $V = \rho g\xi_0$ and the dynamic pressure across the sub-channels is $V_2 = \rho g\xi_2$. The introduction of fence(s) of tidal turbines into Sub-channel 2 augments its resistance by $R_t = \rho\delta|Q_2|$.

The electrical circuit in Figure 3c is now used to determine the power potential of turbines placed in Sub-channel 2. Although this solution is only directly applicable for the multiply-connected channels in Figure 3a, we point out in some practical situations it might be reasonable to reduce more complicated multiply-connected channels with more than two parallel sub-channels (*e.g.* Figure 3b) to the circuit represented by Equation (7). This reduction to an equivalent circuit, which is well-known in electrical circuit theory, requires that a single effective resistance and inductance can be determined for the connecting channel or the principal sub-channels (*i.e.* Sub-channel 2 and 3) if they have secondary sub-channels of their own. Given the non-linearity of the resistors in the context of tidal channels, determination of these effective values is only strictly possible if the flow in the secondary sub-channels is inertia-dominated (for sub-channels without turbines), drag-dominated or when the impedances of the secondary sub-channels are identical. Nevertheless, for more general flow regimes the reduction may still be a very good first approximation. For example this approximation is made implicitly by Draper *et al.* (2013) when comparing the power potential of the entire Pentland Firth (which contains sub-channels) to the single channel model of GC05; leading to good agreement. The approximation was also assumed by Sutherland *et al.* (2008) when comparing the 'One Channel Open' scenario (in which flow still splits into sub-channels in parts of the strait) to the single channel model of GC05; also demonstrating good agreement.

To analyse more complicated multiply-connected channels than those in Figure 3 without the need for approximations (and to recover separate estimates of power extraction in scenarios with more than one deployment of tidal turbines) we introduce a predictive model in Section 3.3.

3.2.1 Approximate solution

As was the case for the single tidal channel, we explore the power potential of the turbines in the equivalent electrical circuit in Figure 3c assuming that the driving tide can be well represented by $\xi_0 = a\cos(\omega t)$ and that this water level difference remains unchanged as tidal turbines are introduced. We also assume that the resistors R_i are independent of flow rate (*i.e.* they are linear). With these assumptions equating the voltage (dynamic pressure) across the sub channels and invoking continuity of the current (flow rate) through the sub-channels leads to

$$I_2 = I - I_3 = I - I_2\frac{Z_2 + R_t}{Z_3}, \tag{8}$$

where $Z_j = \omega L_j + R_j$ is the impedance of the jth section of the channel, and I_2 and I_3 are the currents through Sub-channels 2 and 3, respectively. Applying Kirchhoff's voltage law around the left hand loop in Figure 3c leads to

$$V = I\left(Z_1 + \frac{(Z_2 + R_t)Z_3}{Z_2 + R_t + Z_3}\right). \tag{9}$$

Combining Equations (8) and (9) then gives:

$$I_2 = V\left(\frac{Z_3}{Z_1(Z_2+R_t+Z_3)+(Z_2+R_t)Z_3}\right), \tag{10}$$

and the power extracted by the tidal turbines, averaged over a tidal period, can be written as:

$$\bar{P} = \frac{1}{2}R_t|I_2|^2 = \frac{1}{2}|V|^2 R_t \frac{|Z_3|^2}{|Z_1(Z_2+R_t+Z_3)+(Z_2+R_t)Z_3|^2}. \tag{11}$$

It is easy to show that this has a maximum when $R_t = |Z_1Z_2 + Z_1Z_3 + Z_2Z_3|/|Z_1 + Z_3|$,

$$\bar{P}_{max} = \frac{1}{4}\Gamma\frac{|Z_1Z_2 + Z_1Z_3 + Z_2Z_3|}{|Z_2||Z_1+Z_3|}|V_{2,0}||I_{2,0}|, \tag{12}$$

where the additional subscript '0' again refers to undisturbed quantities before tidal turbines are introduced, and

$$\Gamma^{-1} = 1 + \frac{Re\{(Z_1Z_2 + Z_1Z_3 + Z_2Z_3)/(Z_1+Z_3)\}}{|Z_1Z_2 + Z_1Z_3 + Z_2Z_3|/|Z_1+Z_3|}. \tag{13}$$

We note that this result is identical to that obtained by Cummins (2013) who considered the linear problem in detail. Since the resistances and inductances are all positive (to be physically meaningful) it follows from Equation (13) that $1/2 \le \Gamma \le 1$.

Equation (12) can now be further simplified to give:

$$\bar{P}_{max} = \frac{1}{4}\Gamma|V_{2,0}||I_{2,0}| \times \left(\frac{|I_0|}{|I_{3,0}|}\frac{1}{\left|1+\frac{V_{2,0}}{V_0}\frac{I_{2,0}}{I_{3,0}}\right|}\right). \tag{14}$$

The form of Equation (14) is similar to that of Equation (6) for a single channel with linear resistors. In particular, the power potential is again dependent on (i) a multiplier (now given by $\Gamma/4$), which is again bounded between 0.125 and 0.25 depending on the dynamic balance of the multiply-connected channel, and (ii) the natural undisturbed current and voltage, but this time only across the sub-channel with tidal turbines. However, a key difference between Equation (14) and Equation (6) is the additional term in brackets, which accounts for the presence of the connecting and parallel channels. As expected, this additional term tends to $|V_0|/|V_{2,0}|$ as $I_{2,0}/I_{3,0} \to \infty$ and $I_0/I_{2,0} \to 1$, in which case the bypassing sub-channel vanishes (i.e. its impedance is infinite) and Equation (14) becomes identical to Equation (6). Alternatively, the additional term in brackets tends to 1 in the opposite limit as $I_{2,0}/I_{3,0} \to 0$ and $I_0/I_{3,0} \to 1$, in which case the sub-channel into which tidal turbines are to be added offers little net impedance to the multiply-connected channel and so, as in the case of an isolated channel, the addition of tidal turbines will have little effect on the voltage across the sub-channel (although this voltage is now $V_{2,0}$ and may be small if the impedance in the bypassing sub-channel is small). Finally a third limiting condition (which cannot be directly deduced from (14)) results when $(l_1, l_3) \to 0$ so that the impedance of the connecting channel limits to zero (i.e. $R_1, L_1 \to 0$). Then both sub-channels are effectively uncoupled and $V_{2,0} \equiv V_0$ so that Equation (14) is again equivalent to Equation (6). These three limiting conditions are the same as those examined by Cummins (2013).

Motivated by the close resemblance between the linear and non-linear results for a single tidal channel given in Section 3.1, we now seek solutions for the power potential based on the full non-linear Equation (7), and compare them to the result in Equation (14). Simplifying Equation (7), noting continuity in flowrate, and introducing the non-dimensional parameters $t' = \omega t$, $(\xi', \xi_2') = (\xi, \xi_2)/a$, and $(Q', Q_2', Q_3') = (Q, Q_2, Q_3)\omega c_1/(ga)$ leads to:

$$\begin{bmatrix} \frac{dQ'}{dt'} \\ \frac{dQ_2'}{dt'} \end{bmatrix} = \mathbf{M}^{-1} \begin{bmatrix} \cos(t') - \lambda_1 (Q'|Q'| + \delta_{12}^{-1}(1+\delta_{t2})Q_2'|Q_2'|) \\ \lambda_1 \delta_{12}^{-1}\left((1+\delta_{t2})Q_2'|Q_2'| - \delta_{32}(Q'-Q_2')|Q'-Q_2'|\right) \end{bmatrix}, \tag{15}$$

where

$$\mathbf{M} = \begin{bmatrix} 1 & \frac{1}{L_{12}} \\ \frac{L_{32}}{L_{12}} & -\frac{L_{32}}{L_{12}} - \frac{1}{L_{12}} \end{bmatrix}.$$

This defines a system of ordinary differential equations in terms of six dimensionless parameters

$$L_{12} = \frac{L_1}{L_2}, L_{32} = \frac{L_3}{L_2}, \delta_{12} = \frac{\delta_1}{\delta_2}, \delta_{32} = \frac{\delta_3}{\delta_2}, \delta_{t2} = \frac{\delta}{\delta_2}, \text{and } \lambda_1 = \frac{ga\delta_1}{(\omega c_1)^2}. \tag{16}$$

The first four of these ratios can be interpreted as relative inductance and drag in the circuit, respectively, whilst the last parameter defines the dynamic balance in the multiply-connected channel (with $\lambda_1 \to 0$ implying no natural drag and $\lambda_1 \to \infty$ indicative of quasi-steady drag-dominated conditions, provided δ_{12} and δ_{32} remain finite). The ratio δ_{t2} defines relative drag due to tidal turbines, and in turn the power removed by the turbines.

The system of equations defined by Equation (15) can be solved by standard methods (*e.g.* Runge-Kutta methods) for various choices of $\delta_{t,2}$ to determine the maximum extractable power averaged over a tidal cycle. Based broadly on the form of Equation (14), we choose to write the maximum average power as

$$\bar{P}_{max} = \gamma_3 \frac{Q_p}{Q_{3,p}} \frac{1}{\left(1 + \frac{a_2}{a}\frac{Q_{2,p}}{Q_{3,p}}\right)} \rho g a_2 Q_{2,p}, \tag{17}$$

where γ_3 is a multiplier which is a function of the parameters in Equation (16), and Q_p, $Q_{p,2}$ and $Q_{p,3}$ are the amplitudes of the undisturbed flow rates in the connecting channel and sub-channels 2 and 3, respectively. The parameters a and a_2 are the undisturbed amplitudes of the head difference across the complete multiply-connected channel and the sub-channels, respectively.

Adopting Equation (17), we have calculated the maximum average power and γ_3 for a range of different combinations of the non-dimensional parameters defined in Equation (16). To ensure the combinations of non-dimensional parameters are realistic, each combination has been computed in terms of physical quantities. More specifically, the connecting channel geometry and the sub-channel geometries have been approximated with an effective channel cross-sectional area $A_{e,j}$, effective depth $h_{e,j}$, and effective length $l_{e,j}$ (which can be thought of as actual dimensions for an equivalent rectangular channel), and the bed friction parameter

within each channel has been defined as $C_{d,j}$. The first four dimensionless parameters have thus been calculated as:

$$L_{12} \cong \left(\frac{l_1 + l_3}{l_2}\right)\frac{A_{e,2}}{A_{e,1}}, \qquad L_{32} \cong \frac{A_{e,2}}{A_{e,3}} \cong \left(\frac{A_{e,1}}{A_{e,2}} - 1\right)^{-1}, \qquad \text{and}$$
$$\delta_{12} \cong \left(\frac{A_{e,2}}{A_{e,1}}\right)^2 \left(\frac{C_{d,1}h_{e,2}}{C_{d,2}h_{e,1}}\right)\left(\frac{l_1 + l_3}{l_2}\right), \qquad \delta_{32} \cong \left(\frac{A_{e,1}}{A_{e,2}} - 1\right)^{-2} \left(\frac{C_{d,3}h_{e,2}}{C_{d,2}h_{e,3}}\right). \tag{18}$$

in which it has also been assumed for simplicity that (i) the sub-channels have the same length, (ii) differences in the entrance and exit areas of the connecting channel and sub-channels are negligible, and (iii) the sub-channel effective areas sum to that of the connecting channel. Table 3 lists the different physical ratios ($A_{e,1}/A_{e,2}$, $(l_1 + l_3)/l_2$, $C_{d,1}h_{e2}/C_{d,2}h_{e,1}$, and $C_{d,3}h_{e2}/C_{d,2}h_{e,3}$) that have been used to calculate the range of combinations of non-dimensional parameters via Equation (18). These combinations have then been used together with various values of λ_1 (also listed in Table 3) to calculate γ_3. In total γ_3 has therefore been computed for $3^4 \times 6 = 486$ different combinations of input parameters spanning a realistic range of multiply-connected channel geometries.

Figure 4a presents the computed values of γ_3. It can be seen that the value of γ_3 does not vary significantly despite the wide variation in input parameters outlined in Table 3. A few input combinations give $\gamma_3 > 0.3$, but these cases represent the more extreme geometries for which $A_{e,1}/A_{e,2}$ =1.1 and $(l_1 + l_3)/l_2$=5; *i.e.* a relatively long connecting channel and a free sub-channel that is much narrower than the sub-channel with tidal turbines. For all other cases it appears that a value of $\gamma_3 = 0.22$ (a rough average through the results) is a very good approximation. This implies that Equation (17) with this value for γ_3 may provide a practical extension of Equation (4) for sub-channels connected in parallel to other sub-channels. Conveniently, the application of (17) in practice only requires estimates or measurements of the undisturbed peak flows $Q_p, Q_{p,2}$, and $Q_{3,p}$ and amplitudes a and a_2.

Figure 4b shows the amplitude of the flow rate in the sub-channel with tidal turbines at maximum average power extraction, as a fraction of the undisturbed amplitude, for each set of parameters listed in Table 3. It can be seen that the ratio of flow at maximum power extraction is reasonably well-bounded between ~0.5 and ~0.7. A similar small variation in the relative flow rate at maximum power extraction has also been noted by Cummins (2013) who used it to form a prediction of the power potential of parallel-connected sub-channels which terminate in an enclosed bay. Cummins' result is broadly consistent with the findings given in the present paper. However, as noted in the Introduction, Equation (17) can be used directly to estimate power potential, provided measurements of the natural tidal hydrodynamics are available. It does not necessarily require any estimate of the channel geometry or bed friction coefficient, which might be difficult to determine.

3.2.2 Quasi-steady solution

In the case of a drag-dominated multiply-connected channel ($\lambda_1 \to \infty$), the flow through the channel will be quasi-steady and it is then possible to solve Equation (7), and the instantaneous power, algebraically. This solution for a tidal channel that splits into two sub-channels was first discussed by Atwater and Lawrence (2010), and can be written as (noting that the power is normalised herein by a slightly different metric to that used by Atwater and Lawrence (2010))

$$\frac{P}{\rho g \xi_{2,0} Q_{2,0}} = \delta_{t2} \frac{\left(\left(1 + 1/{\delta_{32}}^{1/2}\right)^2 + 1/\delta_{12}\right)^{3/2}}{\left(\left(1 + (1+\delta_{t2})^{1/2}/{\delta_{32}}^{1/2}\right)^2 + (1+\delta_{t2})/\delta_{12}\right)^{3/2}}. \quad (19)$$

where $\xi_{2,0}$ and $Q_{2,0}$ are the elevation difference and flow rate at any instant in the absence of turbines. Extracting power also leads to a reduction in flow rate through the sub-channel with turbines, such that

$$\frac{Q_2}{Q_{2,0}} = \frac{\left(\left(1 + 1/{\delta_{32}}^{1/2}\right)^2 + 1/\delta_{12}\right)^{1/2}}{\left(\left(1 + (1+\delta_{t2})^{1/2}/{\delta_{32}}^{1/2}\right)^2 + (1+\delta_{t2})/\delta_{12}\right)^{1/2}}. \quad (20)$$

Equation (19) has a maximum as δ_{t2} is varied, which is dependent on δ_{12} and δ_{32}. This maximum (denoted as γ_s) can be found numerically. Furthermore, if $\xi_{2,0} = a_2 \cos(\omega t)$, as is the case if there is a sinusoidal variation in the elevation difference across the entire multiply-connected quasi-steady channel, the flow rate in the sub-channel with turbines can be written as $Q_{2,0} = Q_{p,2} |\cos(\omega t)|^{1/2}$. Therefore the maximum power that can be extracted (averaged over a tidal cycle) is simply $\bar{P}_{max} = 0.56 \gamma_S \rho g a_2 Q_{p,2}$ (where the factor 0.56 arises from averaging $|\cos(\omega t)|^{3/2}$ over a tidal cycle; see GC05). This result for the maximum average power is presented in Figure 5a for $\lambda_1 \to \infty$. The corresponding change in flow rate at peak extraction, from Equation (20), is also plotted in Figure 5b.

3.2.3 Application to the Pentland Firth

We now investigate how well Equation (17) (with $\gamma_3 = 0.22$) agrees with the 2D numerical model results for the Pentland Firth documented in Draper *et al.* (2013). To do this we assume that the equivalent circuit in Figure 3c is appropriate for Cases A, B, C, D and E, and for Cases BC, BD and CD (*i.e.* that Channels B, C and D are all in parallel). The undisturbed flow rate amplitudes Q_p, $Q_{2,p}$ and $Q_{3,p}$ are obtained from the numerical model results, where $Q_{2,p}$ is the sum of the flow rates in two sub-channels in Cases BC, BD and CD, and $Q_{3,p}$ is the sum of the flow rates in two sub-channels in Cases B, C and D. The dynamic head across the entire Pentland Firth is taken to be a = 1.32 m (Draper *et al.* 2013) and, as in the theory, we assume that this remains fixed with the addition of tidal turbines. Results given by Draper *et al.* 2013 (see also Table 2) suggest that this is a reasonable assumption, since changes in a are less than 8 % for all cases except CD (for which the change is 16%). Lastly the dynamic head across the sub-channels is calculated from the elevation difference between locations P_3 and P_4, or P_5 and P_6 for case E (see Figure 1 for the locations of points P_1 to P_6). These elevation differences are close to sinusoidal in time (see Figure 5) and have amplitudes of 0.53 m and 0.26 m, respectively.

Table 4 summarises the input values and compares the predictions using Equation (17) with the 2D numerical model results. In general there is reasonable agreement, with predictions based on the expected value of a_2 in agreement to within 20 % of the 2D numerical model results for all cases. Furthermore, in all cases except CD Equation (17) gives a result that is significantly better than that obtained using Equation (4) (using the peak flow rate for the sub-channel(s), the dynamic head for the entire Pentland Firth and γ =0.22), which ignores

the interaction effects of the sub-channels and the ability of the flow to divert through different sub-channels.

In practice, of the five variables that must be estimated to use Equation (17), the variable a_2 is perhaps the most difficult to select. This is because a_2 should be calculated using points located immediately either side of the sub-channels where the mean elevation difference laterally across the channel is small. Since these locations are often hard to define, upper and lower bound estimates of a_2 have been considered herein by taking the locations P_3 to P_6 to be any locations within the circular regions shown in Figure 1b. Power estimates using these upper and lower bound values are also given in Table 4, from which it can be observed that variations in a_2 can lead to significant variations in power predictions. However, for the bound values considered, the predictions made using Equation (17) are still in much better agreement with the 2D numerical model results than the predictions given by Equation (4).

Finally we note that in Table 2 the numerically predicted amplitude of flow rate at maximum extraction, relative to that in the natural state, is within the range displayed in Figure 4b.

3.3 Tidal fences placed in series and parallel

So far the electrical analogy has been used to review single tidal channels and to analyse a multiply-connected channel in which tidal turbines are installed in a parallel sub-channel. We now consider the more general case of tidal turbines installed in series and parallel within a more complicated multiply-connected channel system. In this case there are many different combinations of channel arrangements and so it is not practical to determine approximate analytical solutions for all arrangements. Instead, a simple predictive model is constructed based on an equivalent electrical circuit for the Pentland Firth, and each of the inductors and resistors in the circuit are calibrated using measurements of undisturbed flow and dynamic head across various sections of the Firth. It should be noted that although the predictive model is applied to the Pentland Firth herein, a similar model could also be devised for other multiply-connected channels.

Figure 6 shows the equivalent electrical circuit for the Pentland Firth, which includes two parallel branches in series with the connecting channel. The first parallel branch has three sub-channels representing Sub-channels B, C and D, which are separated by the islands of Stroma and Swona, and the second parallel branch has two sub-channels representing passage E and a second passage denoted F, which is bordered by the Pentland Skerries and the Scottish mainland. There is a voltage drop (or dynamic pressure) across the two parallel branches of V_2 and V_3, respectively, and within each sub-channel there is a resistor and inductor which describe the impedance of the sub-channels. The connecting channel accounts for the channel's net impedance over and above that due to sub-channels (i.e. all locations along the channel between the branches of sub-channels). The total voltage (or dynamic pressure) across the circuit (multiply-connected channel) is V.

To simplify our equivalent network, impedance associated with the body of water to the north of Swona is neglected, since the flow rate into and out of this region is relatively small. Radiation impedance for the connecting channel is also ignored because it is unlikely to have an effect on the assumed driving voltage unless the flow through the circuit (*i.e.* Pentland Firth as a whole) significantly reduces. This is not expected in scenarios where sub-channels with significant relative cross-sectional area do not contain tidal turbines (and indeed the change was less than 20 % for all cases modelled by Draper *et al.* (2013); see also Table 2).

To use the equivalent circuit it is first necessary to calibrate the different electrical components. For the sub-channels, using the same assumptions outlined in Section 3.1, the dynamic balance across each sub-channel leads to

$$V_k = L_{k,j}\frac{dI_j}{dt} + \rho\delta_{k,j}|I_j|I_j, \tag{21}$$

where $V_k \equiv \rho g\, \xi_k$ and $I_j \equiv Q_j$, and the subscripts j and k represent the jth sub-channel within the kth branch of parallel sub-channels. Now, if the driving voltage and current through each sub-channel are almost sinusoidal, so that $V_k \sim Re\{|V_k|e^{i(\omega t+\alpha)}\} = \rho g a_k \cos(\omega t+\alpha)$, and $I_j \sim Re\{|I_j|e^{i(\omega t+\beta)}\} = Q_{j,p}\cos(\omega t+\beta)$, where ω is the angular frequency of the tidal constituent and α and β are phase lags, the non-linear term $|I_j|I_j$ in (21) can be reasonably well approximated by the first term in its Fourier series. Equation (21) can then be rewritten approximately as,

$$V_k \cong I_j\left(i\omega L_{k,j} + \frac{8}{3\pi}\rho\delta_{k,j}|I_j|\right). \tag{22}$$

Hence, provided V_k and I_j can be measured, the parameters describing resistance and inductance can be calibrated simply as:

$$\delta_{k,j} \cong \frac{3\pi}{8\rho|I_j|}Re\left\{\frac{V_k}{I_j}\right\} \quad \text{and} \quad L_{k,j} \cong \frac{1}{\omega}Im\left\{\frac{V_k}{I_j}\right\}. \tag{23}$$

Replacing the voltage and current with dynamic pressure and flow rate, Equation (23) is equivalent to:

$$\delta_{k,j} \cong \frac{3\pi g\, a_k}{8Q_{j,p}^2}\cos(\alpha-\beta) \quad \text{and} \quad \rho c_{k,j} \cong \frac{\rho g a_k}{\omega Q_{j,p}}\sin(\alpha-\beta). \tag{24}$$

The resistance and inductance of the connecting channel (denoted by subscript A) can also be calibrated. In this case the dynamical balance across the entire multiply-connected channel can be written as:

$$V - V_2 - V_3 = L_A\frac{dI_A}{dt} + \rho\delta_A|I_A|I_A, \tag{25}$$

so that, following the logic for the sub-channels,

$$\delta_A = \frac{3\pi}{8\rho|I_A|}Re\left\{\frac{V-V_2-V_3}{I_A}\right\} \quad \text{and} \quad L_A = \frac{1}{\omega}Im\left\{\frac{V-V_2-V_3}{I_A}\right\}. \tag{26}$$

Or, introducing dynamic pressure and flow rate

$$\delta_A \cong \frac{3\pi g a_A}{8{Q_{A,p}}^2}\cos(\sigma-\psi) \quad \text{and} \quad L_A \cong \frac{\rho g a_A}{\omega Q_{A,p}}\sin(\sigma-\psi), \tag{27}$$

where $\xi - \xi_2 - \xi_3 \cong a_A\cos(\omega t+\sigma)$ and $Q_A \cong Q_{A,p}\cos(\omega t+\psi)$.

3.3.1 Calibrating the Pentland Firth

Figure 5 illustrates the dynamic head difference across the Pentland Firth and both branches of sub-channels (approximated as the elevation difference between points P_3 and P_4, and P_5 and P_6, respectively) over a tidal period when the numerical model is forced solely by the M2 tidal constituent. Assuming that these elevation differences are sufficiently sinusoidal Equations (24) and (27) can be used to calibrate each of the elements in the electrical circuit of Figure 6.

To perform the calibration we first estimate the dynamic head across the entire Firth and the two branches of sub-channels using the simulated elevation differences at points P_1 through P_6 in the 2D numerical model. This leads to

$$\xi_0 = 1.32\cos(\omega t), \qquad \xi_2 = 0.53\cos(\omega t + 38.5^{\circ}), \quad \xi_3 = 0.26\cos(\omega t + 41.9^{\circ}), \tag{28}$$

where $\omega = 0.00014$ rad/s for the M2 tide, and the phase difference of the dynamic head across the branches of sub-channels has been computed relative to the dynamic head across the entire Pentland Firth (calculated between points P_1 and P_2). Similarly, estimates of the flow rates through the entire Pentland Firth and the various sub-channels are obtained from the numerical model; the resulting flow rates and phase lags are given in the second and third columns in Table 5, respectively. Using these inputs, the predicted inductance and resistance for each circuit component are computed from Equation (24) and (27) and listed in the fourth and fifth columns of Table 5.

The equivalent circuit can now be used to examine the power that can be extracted by placing tidal turbines in parallel and series across various sub-channels. For example, consider two separate deployments of tidal turbines in sub-channels B and E, which are represented by the two additional resistors $R_{t,1} = \rho\delta_{t,1}|Q_B|$ and $R_{t,2} = \rho\delta_{t,2}|Q_E|$ in the equivalent circuit (as shown in Figure 6). The dynamic model describing the equivalent circuit can now be written, using Kirchoff's laws, as a system of ordinary differential equations. For example:

$$\begin{bmatrix} \frac{dQ}{dt} \\ \frac{dQ_B}{dt} \\ \frac{dQ_C}{dt} \\ \frac{dQ_E}{dt} \end{bmatrix} = \mathbf{M}^{-1} \begin{bmatrix} \rho g a_A \cos(\omega t) - \left(\rho\delta_A Q_A|Q_A| + \rho(\delta_{t,1} + \delta_B)Q_B|Q_B| + \rho(\delta_{t,2} + \delta_E)Q_E|Q_E|\right) \\ \rho\delta_C Q_C|Q_C| - \rho(\delta_{t,1} + \delta_B)Q_B|Q_B| \\ \rho\delta_D(Q - Q_B - Q_C)|Q - Q_B - Q_C| - \rho(\delta_{t,1} + \delta_B)Q_B|Q_B| \\ \rho\delta_F(Q - Q_E)|Q - Q_E| - \rho(\delta_{t,2} + \delta_E)Q_E|Q_E| \end{bmatrix}, \tag{29}$$

where

$$\mathbf{M} = \begin{bmatrix} L_A & L_B & 0 & L_E \\ 0 & L_B & -L_C & 0 \\ -L_D & L_B + L_D & L_D & 0 \\ -L_F & 0 & 0 & L_E + L_F \end{bmatrix},$$

and the average power extracted by the two deployments of tidal turbines, for a given choice of $\delta_{t,1}$ and $\delta_{t,2}$, is given by $\bar{P} = \left(\int^T \{\rho\delta_{t,1}|Q_B|^3 + \rho\delta_{t,2}|Q_E|^3\}\, dt\right)/T$.

To confirm that the calibrated inductors and resistors lead to the same flow rates as predicted by the 2D numerical model we first solve Equation (29) for $\delta_{t,1} = \delta_{t,2} = 0$. The final two columns of Table 5 show that there is reasonable agreement. Next, the system is solved for numerous combinations of $\delta_{t,1}$ and $\delta_{t,2}$ in order to determine the maximum extracted power

averaged over a tidal cycle. This calculation is repeated for turbines placed concurrently in sub-channels C and E, and D and E, respectively. Table 6 summarises the power estimates and predicted flow rates at maximum power extraction and compares them with the 2D numerical model. There is reasonable agreement between the estimates, with at most only 29% and 19% differences between the equivalent circuit model and the 2D numerical model for predictions of maximum average power and flow rate, respectively.

It should be noted that the values of the inductors and resistances in the equivalent circuit are sensitive to the flow and dynamic head estimates used for calibration. As for parallel-connected channels, perhaps the most uncertain of these estimates is the dynamic head across the parallel sub-channels. To investigate further the sensitivity to the choice of this input, Table 6 also gives upper and lower bound predictions from the equivalent circuit model when ξ_2 and ξ_3 are calculated using any points within the circles drawn in Figure 1b. Across these bound values the agreement is within 45% for the power prediction and within 37% for prediction of flow rate. These estimates agree less well with the numerical model, but they are nevertheless useful given that there is currently no other simple and straightforward means to estimate the combined power potential of tidal turbines placed in parallel and series within a multiply-connected channel.

4. Discussion

An equivalent electric circuit analogy has been used to unlock some of the complexity in predicting the power that can be extracted by tidal turbines placed within multiply-connected channels. This analogy has led to the development of a simple predictive formula, Equation (17), which is in broad agreement with that given by Cummins (2013) but can be used to assess the power potential of turbines deployed in a sub-channel connected in parallel to another sub-channel using only measurements of natural tidal hydrodynamics. The formula has been shown to give predictions in reasonable agreement with results from a depth-averaged numerical model of the Pentland Firth, and this indicates that Equation (17) could be used to provide an initial tidal resource assessment of other multiply-connected channels with parallel sub-channels. Indeed its performance is likely to be much better than Equation (4).

The equivalent electric circuit analogy can also be applied to complicated scenarios, in which tidal turbines may be placed in series and parallel across different sub-channels of a multiply-connected channel. Herein, an equivalent circuit was developed for the Pentland Firth and the inductors and resistors within the circuit were calibrated using measurements of the natural tidal hydrodynamics. The effect of adding tidal turbines (*i.e.* resistors) to this multiply-connected channel system (*i.e.* equivalent circuit) was then examined by solving a system of ordinary differential equations describing the circuit. Reasonable agreement was obtained between the power estimates obtained using the simplified electric circuit model and those from the 2D numerical shallow flow solver for the Pentland Firth. This provides confidence in the model and also provides insight into the dynamics of tidal flow in the Pentland Firth and the tidal resource more generally.

Finally, as pointed out by Draper *et al.* (2013) and Adcock *et al.* (2013) it should be noted that the estimates in Table 1 are only upper bounds to power generation. The useful power that can be removed by tidal turbines from a multiply-connected tidal channel such as the Pentland Firth will be necessarily lower due to environmental constraints and the fact that tidal turbines are not perfectly efficient based on hydrodynamic arguments alone. In the latter case, linear momentum actuator disc theory or a similar model could be used to represent

turbines so as to give a better estimate of the useful (or available) power for generation (see, for example, Houlsby *et al.* (2008), Vennell, (2010) and Adcock *et al.* (2013)). Importantly, the use of a predictive model based on an equivalent electrical circuit could be used to represent the multiply-connected channel in this exercise providing a more efficient means to account for the interaction between turbine deployments in different sub-channels than more computationally demanding 2D or 3D numerical models.

Acknowledgements

The authors would like to thank one reviewer for several comments that have significantly improved this paper. The first author is a member of the Centre for Offshore Foundation Systems (COFS), currently supported as a node of the Australian Research Council Centre of Excellence for Geotechnical Science and Engineering, and is thankful for support by the Lloyds Register Foundation. The second author was supported by the PerAWaT project sponsored and commissioned by the Energy Technologies Institute, UK.

References

Adcock, T. A. A., Draper, S., Houlsby, G. T., Borthwick, A. G. L., and Serhadlioglu, S. (2013), "The available power from tidal stream turbines in the Pentland Firth", Proceedings of the Royal Society, Part A, 469:20130072.

Atwater, J.F. and Lawrence, G.A. (2010), "Power potential of a split tidal channel", Renewable Energy, 35, pp. 329-332.

Crown Estate (2011), "Wave and tidal energy in the Pentland Firth and Orkney Waters: How the project could be built." Tech. rep., prepared by BVG Associates. Accessed from http://www.thecrownestate.co.uk/energy/wave-and-tidal/ on 1/07/2012.

Cummins, P.F. (2013), "The extractable power from a split tidal channel: An equivalent circuit analysis", Renewable Energy, 50, pp. 395-401.

Draper, S., Adcock, T.A.A., Borthwick, A.G.L. and Houlsby, G.T. (2013) "Estimate of the Extractable Pentland Firth Tidal Stream Power Resource", Renewable Energy (Accepted, In Press).

DTI (2004), Atlas of UK Marine Renewable Energy Resources. Tech. Rep. R. 1106. Department of Trade and Industry.

Garrett, C. & Cummins, P. (2005); "The power potential of tidal currents in channels". Proceedings of the Royal Society London A, 461, pp.2563-2572.

Houlsby, G.T., Draper, S. and Oldfield, M.L.G. (2008). "Application of linear momentum actuator disc theory to open channel flow. Report No. OUEL 2296/08, Department of Engineering Science, University of Oxford.

Lighthill, J., (1878) "Waves in Fluids", Cambridge University Press.

Miles, J.W. (1971), "Resonant response of harbours: an equivalent-circuit analysis", Journal of Fluid Mechanics, 46, pp. 241-265.

Polagye, B.L. and Malte, P.C. (2011), "Far-field dynamics of tidal energy extraction in channel networks", Renewable Energy, vol. 36, pp. 222-234.

Rainey, R.C.T., (2009), "The optimum position for a tidal power barrage in the Severn estuary", Journal of Fluid Mechanics, 636, pp. 497-507.

Sutherland, G., Foreman, M. & Garrett, C., (2007), "Tidal current energy assessment for Johnstone Strait, Vancouver Island." Proceedings of the Institution of Mechanical Engineers, Part A: Journal of Power and Energy, 221(2), pp. 147–157.

Vennell, R., (2010), Tuning Turbines in a Tidal Channel, Journal of Fluid Mechanics, 663, 253-267.

Vennell, R. (2011), "Estimating the Power Potential of Tidal Currents and the Impact of Power Extraction on Flow Speeds", Renewable Energy, 36, pp. 3558-3565.

Tables

Table 1: Maximum averaged extracted power for various combinations of tidal deployments in the Pentland Firth. A* is calculated with M2 and S2 tidal forcing at the boundary of the numerical model, all other values are with M2 tidal forcing only. Reproduced from Draper *et al.* (2013).

Case	Locations modelled (Maximum power extraction, MW)					Total Power Extracted (MW)
	A	B	C	D	E	
A	3748	-	-	-	-	3748
A*	4187	-	-	-	-	4187
BCD	-	320	2371	1087	-	3779
B	-	122	-	-	-	122
C	-	-	1420	-	-	1420
D	-	-	-	388	-	388
E	-	-	-	-	325	325
BC	-	217	1520	-	-	1737
BD	-	148	-	412	-	560
CD	-	-	2228	1000	-	3228
BE	-	108	-	-	314	422
CE	-	-	1310	-	213	1523
DE	-	-	-	316	284	600

Table 2: M2 amplitude in flow rate through the entire Pentland Firth (at A) and the sub-channels (B, C, D and E) at maximum power extraction, as a fraction of natural undisturbed M2 amplitude in flow rate. Values in bold are the locations where tidal turbines are deployed. Final column gives the change in amplitude of the elevation difference between points P_1 and P_2 at maximum power extraction (defined as a), relative to that in the natural state. (Note: * value rounded up from 0.996). Reproduced from Draper *et al.* (2013).

Case	A	B	C	D	E	Change in, a
A	**0.58**	0.59	0.58	0.59	0.69	+ 17 %
B	1.00*	**0.56**	1.02	1.02	1.00	+ 0.0 %
C	0.84	1.24	**0.53**	1.45	0.85	+ 6.7 %
D	0.97	1.09	1.14	**0.50**	0.95	+ 1.6 %
E	0.96	0.96	0.97	0.95	**0.58**	+ 1.4 %
BC	0.82	**0.63**	**0.56**	1.64	0.94	+ 8.0 %
BD	0.96	**0.58**	1.29	**0.58**	1.10	+ 2.2 %
CD	0.68	1.52	**0.59**	**0.62**	0.75	+ 16 %
BE	0.94	**0.54**	0.98	0.95	**0.46**	+ 2.2 %
CE	0.82	1.20	**0.54**	1.40	**0.53**	+ 9.4 %
DE	0.92	1.03	1.09	**0.47**	**0.50**	+ 5.3 %
BCD	0.61	**0.57**	**0.56**	**0.61**	0.67	+ 17 %

Table 3: Parameter range explored for the multiply-connected channel with turbines installed in a parallel sub-channel.

$A_{e,1}/A_{e,2}$	$(l_1 + l_3)/l_2$,	$C_{d,1}h_{e2}/C_{d,2}h_{e,1}$,	$C_{d,1}h_{e2}/C_{d,2}h_{e,1}$	λ_1
1.1, 2, 10	0.2, 1, 5	0.5, 1, 2	0.5, 1, 2	1, 2.5, 5, 10, 100, 200, ∞

Table 4: Comparison of maximum power predicted by numerical model with that by Equation (17) and Equation (4). For a_2 an expected value (Ex.), upper bound (UB) and lower bound (LB) are given. The UB and LB are selected by considering all points within a 1.5 km radius of P_3 and P_4 and 750 m radius of P_5 and P_6 (for Case E) defined in Figure 2. Numbers in bold are percentage differences with the model results in Table 1.

Case	Inputs							Predicted Power Potential, $\bar{P}_{max}$				
	Q_p	$Q_{2,p}$	$Q_{3,p}$	a	a_2			Eq. (17)			Eq. (4)	Table 1
	10^6 m^3/s			m	m			MW			MW	MW
					LB	UB	Ex.	LB.	UB	Ex.		
A	1.17	1.17	0.00	1.32	NA	NA	NA	NA	NA	3423 **9%**	3031	3748
B	1.17	0.08	1.09	1.32	0.51	0.63	0.53	94	116	98 **20%**	234	122
C	1.17	0.76	0.40	1.32	0.51	0.63	0.53	1449	1628	1481 **4%**	2223	1420
D	1.17	0.32	0.84	1.32	0.51	0.63	0.53	439	527	454 **17%**	936	388
E	1.17	0.34	0.80	1.32	0.21	0.30	0.53	217	302	264 **18%**	995	325
BC	1.17	0.84	0.32	1.32	0.51	0.63	0.53	1724	1904	1757 **1%**	2458	1737
BD	1.17	0.40	0.76	1.32	0.51	0.63	0.53	578	687	597 **7%**	1170	560
CD	1.17	1.09	0.08	1.32	0.51	0.63	0.53	2877	2967	2894 **10%**	3190	3228

Table 5: Calibration of parameters to define inductance and resistance for the different elements in the equivalent electrical circuit used to describe the Pentland Firth. Comparison of simulated undisturbed flow rates is also made between the equivalent electric circuit model and the 2D depth-averaged model. Note: the phase is the phase lag relative to the dynamic head across the entire Pentland Firth.

Channel	2D numerical model		Inductance, $L_{k,j}$	Drag, $\delta_{k,j}$	Equivalent electric circuit model	
	$Q_{j,p}$	Phase lag	kg m^{-4}	10^6 kg m^{-7}	$Q_{j,p}$	Phase lag
	10^6 m^3/s	deg.			10^6 m^3/s	deg.
Connecting Channel	1.17	49.6	29.9	2.06	1.15	50.6
Sub-channel B	0.08	37.0	200	824	0.08	37.4
Sub-channel C	0.76	50.3	31.4	8.31	0.75	50.2
Sub-channel D	0.32	55.3	81.4	42.5	0.32	55.0
Sub-channel E	0.34	43.1	30.4	20.7	0.34	42.8
Sub-channel F	0.80	55.1	16.4	3.12	0.81	54.0

Table 6: Power estimates from the simplified electrical circuit model, compared with the 2D depth-averaged numerical model. An expected value (Ex.), upper bound (UB) and lower bound (LB) are selected by considering all points within a 1.5 km radius of P_3 and P_4 and 750 m radius of P_5 and P_6 (for Case E) defined in Figure 2, to calibrate the equivalent circuit.

Case		Maximum Average Power (MW)				M2 amplitude in flow rate at maximum extraction (10^6 m^3/s)			
		Electrical model simulated results			2D numerical model	Electrical model simulated results			2D numerical model
		LB	UB	Ex.		LB	UB	Ex.	
BE	B	69	103	83 **23%**	108	0.039	0.051	0.043 **2%**	0.042
	E	186	270	223 **29%**	313	0.164	0.209	0.180 **17%**	0.154
CE	C	1069	1536	1262 **4%**	1310	0.362	0.470	0.411 **2%**	0.401
	E	187	270	223 **5%**	213	0.176	0.221	0.194 **9%**	0.178
DE	D	318	442	386 **22%**	316	0.154	0.204	0.177 **19%**	0.149
	E	187	270	223 **21%**	284	0.166	0.216	0.188 **12%**	0.168

Figures

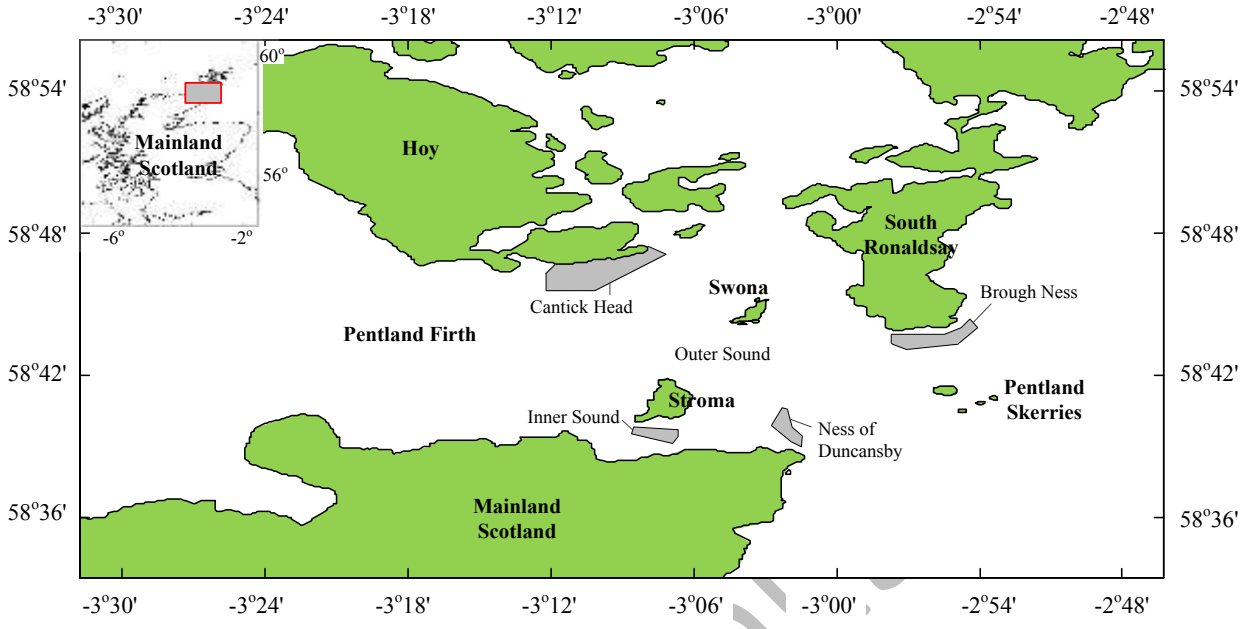

(a)

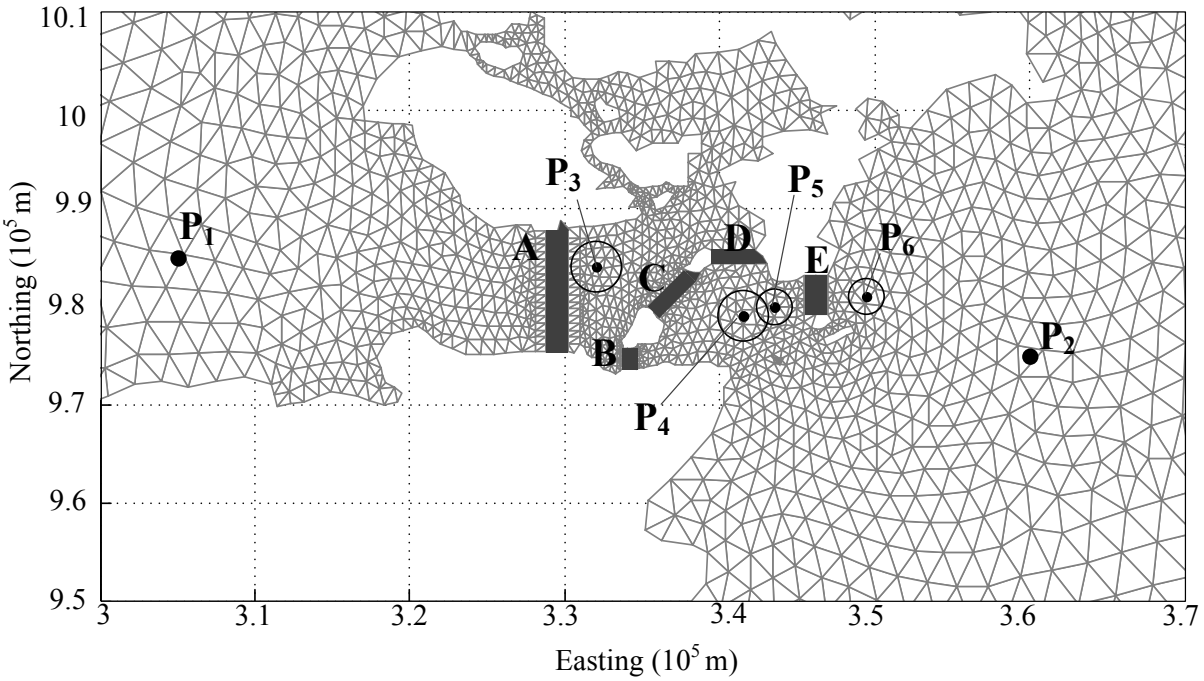

(b)

Figure 1: (a) Numerical mesh used in the hydrodynamic model presented in Draper *et al.* (2013); main geographic features labelled. Shaded polygons indicate sites earmarked by the Crown Estate (2011). (b) Locations A to E where tidal turbines are placed within the Pentland Firth (see Table 1 for power estimates). Point locations in British Grid Easting and Northings (units of km) are: P_1 (305,985); P_2 (360,975); P_3 (332,983); P_4 (341.5,979); P_5 (343.5,980); P_6 (349.5,981). Figure adapted from Draper *et al.* (2013).

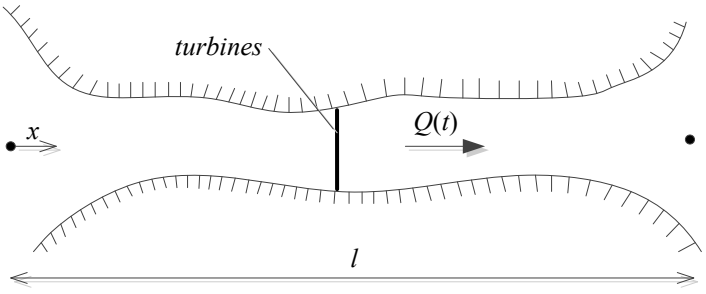

(a)

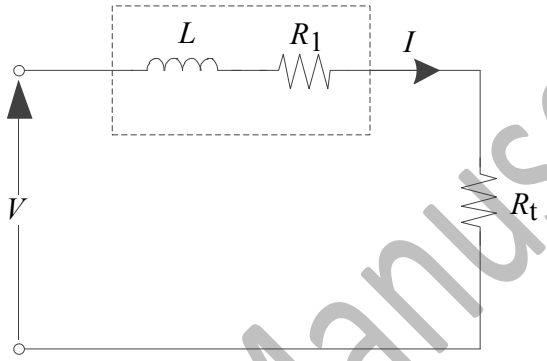

(b)

Figure 2: Single tidal channel and equivalent electric circuit. Dashed box highlights the natural channel elements.

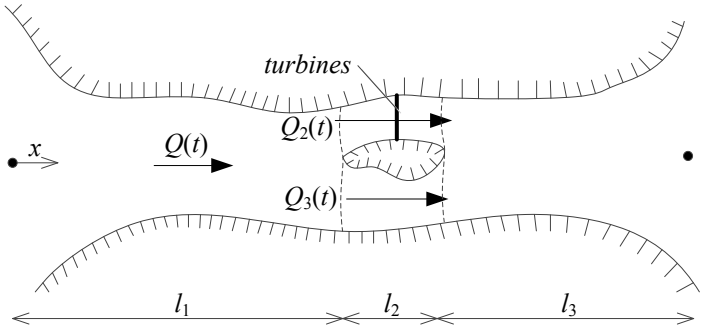

(a)

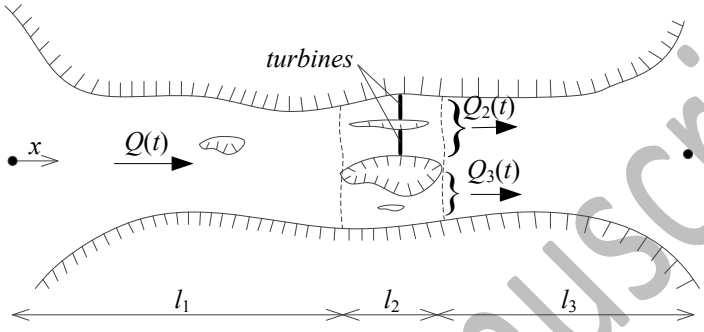

(b)

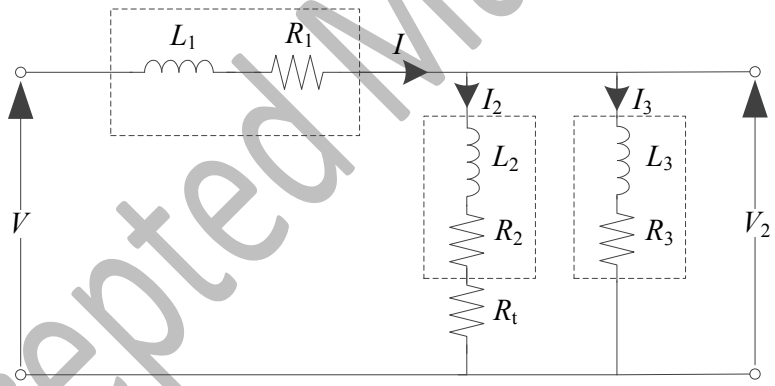

(c)

Figure 3: Multiply-connected tidal channel and equivalent electric circuit. Dashed boxes highlight natural channel elements.

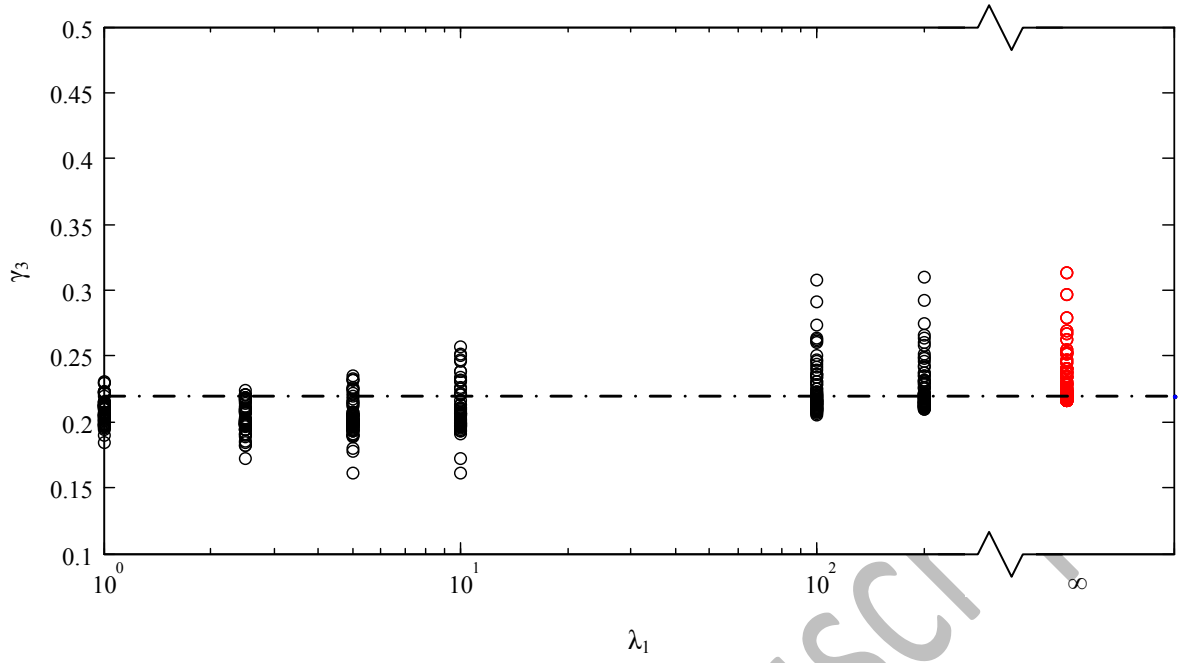

(a)

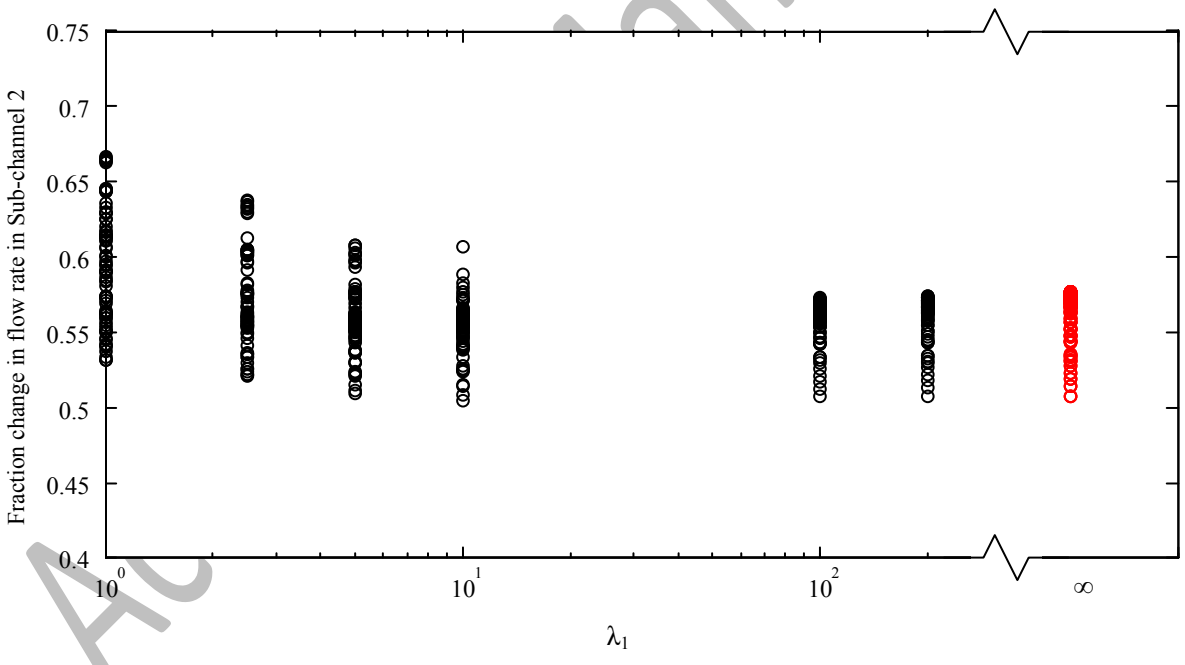

(b)

Figure 4: Results for the different parameters given in Table 3: (a) variation in γ_3, and (b) ratio of peak flow rate in sub-channel 2 at maximum power extraction, compared with that in the natural state, plotted against the non-dimensional parameter λ_2.

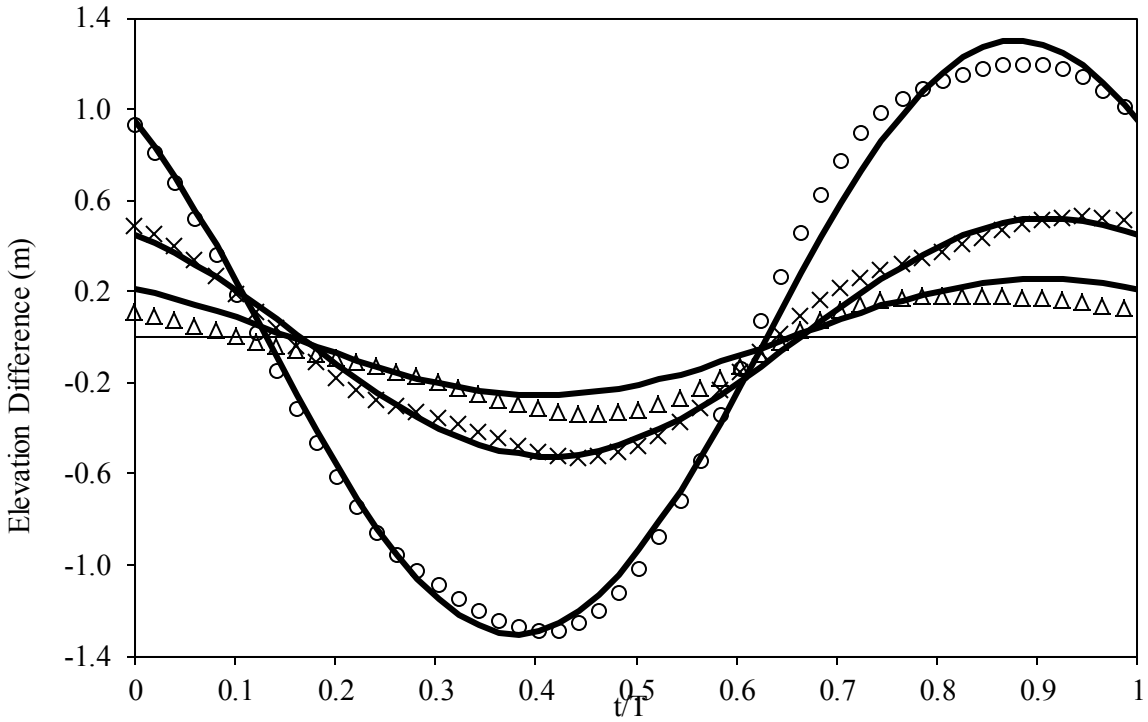

Figure 5: Elevation difference calculated between: o, location P_1 minus P_2; ×, location P_3 minus P_4; Δ, location P_5 minus P_6. (All locations shown in Figure 1b). Solid lines are M2 components.

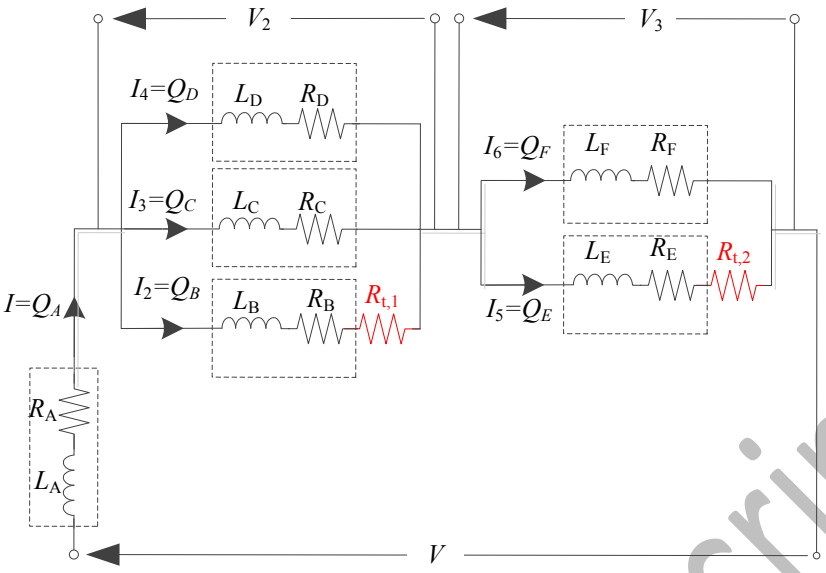

Figure 6: Equivalent circuit for the Pentland Firth. Additional resistors $R_{t,1}$ and $R_{t,2}$ describe deployments of turbines (shown in Sub-channel B and Sub-channel E, as an example).